Annals of Biomedical Engineering, Vol. 45, No. 2, February 2017 (© 2016) pp. 413–426
DOI: 10.1007/s10439-016-1778-0

The Pursuit of Engineering the Ideal Heart Valve Replacement or Repair

A Tri-Leaflet Nitinol Mesh Scaffold for Engineering Heart Valves

S. Hamed Alavi,[1,2] Marc Soriano Baliarda,[3] Noemi Bonessio,[3] Lorenzo Valdevit,[3] and Arash Kheradvar[1,2,3]

[1]The Edwards Lifesciences Center for Advanced Cardiovascular Technology, University of California, Irvine, 2400 Engineering Hall, Irvine, CA 92697-2730, USA; [2]Department of Biomedical Engineering, University of California, Irvine, 3120 Natural Sciences II, Irvine, CA 92697-2715, USA; and [3]Department of Mechanical and Aerospace Engineering, University of California, Irvine, 4200 Engineering Gateway, Irvine, CA 92697-3975, USA

(*Received 6 July 2016; accepted 9 December 2016; published online 22 December 2016*)

Associate Editor Jane Grande-Allen oversaw the review of this article.

Abstract—The epidemiology of valvular heart disease has significantly changed in the past few decades with aging as one of the main contributing factors. The available options for replacement of diseased valves are currently limited to mechanical and bioprosthetic valves, while the tissue engineered ones that are under study are currently far from clinical approval. The main problem with the tissue engineered heart valves is their progressive deterioration that leads to regurgitation and/or leaflet thickening a few months after implantation. The use of bioresorbable scaffolds is speculated to be one factor affecting these valves' failure. We have previously developed a non-degradable superelastic nitinol mesh scaffold concept that can be used for heart valve tissue engineering applications. It is hypothesized that the use of a non-degradable superelastic nitinol mesh may increase the durability of tissue engineered heart valves, avoid their shrinkage, and accordingly prevent regurgitation. The current work aims to study the effects of the design features on mechanical characteristics of this valve scaffold to attain proper function prior to *in vivo* implantation.

Keywords—Nitinol mesh, Heart valve, Scaffold, Non-degradable, Hybrid heart valve, Hybrid tissue engineering approach, Computational modeling.

INTRODUCTION

The prevalence of valvular heart disease (VHD) in the United States has increased to 2.5% with no significant gender difference among the aging population.[24] Dysfunctional valves may be replaced to reduce the associated mortality and morbidity; however, the current replacement options are associated with either potential life threatening drawbacks such as mechanical valves' thrombogenicity or bioprosthetic valves' limited durability. Tissue engineered heart valves (TEHVs) have the potential to resolve these issues and provide self-regeneration either through classical or the newly introduced *in situ* and off-the-shelf approaches.[16] In traditional methods, the valves are implanted with the cells that are seeded in a scaffold pre-implantation. Alternatively, more recent approaches suggest the valve (or scaffold) to be implanted without prior cell-seeding, only relying on recruitment and infiltration of the host's cells that produce extracellular matrix (ECM) and circulating monocytes for eventual tissue remodeling and regeneration.[16,23]

Even though the concept of TEHV is promising, current *in vivo* animal studies have faced long-term functionality hurdles that led to limited durability and progressive regurgitation or stenosis.[9,12,15,32–34,37,40] Although each group uses a distinctive method to develop a TEHV, the use of resorbable scaffolds—either polymeric[9,15,27,30,32,37] or biologic[12,27,30,39]—is shared among them all. These scaffolds are aimed to be degraded over time once the process of host cell invasion occurs. However, this degradation has so far resulted in either leaflet retraction due to the recruitment of α-smooth muscle actin (α-SMA)-expressing cells or leaflet thickening due to excessive ECM production and cellular ingrowth.[16] While this process can be delayed by modifying the rate of scaffold degradation,[5] presence of progressive regurgitation and stenosis at early stages of implantation usually within the first

Address correspondence to Arash Kheradvar, The Edwards Lifesciences Center for Advanced Cardiovascular Technology, University of California, Irvine, 2400 Engineering Hall, Irvine, CA 92697-2730, USA. Electronic mail: arashkh@uci.edu

year is concerning. Although there are alternative methods under investigation to avoid this,[31] we believe using a non-degradable scaffold with proper mechanical properties may address many concerns associated with the degradable ones.

Mesh-enclosed hybrid heart valves that aim for superior durability due to their non-degradable scaffold were first introduced by Alavi and Kheradvar[1–3] and recently adopted by few other groups.[21,28] These valves can be suitable alternatives for current mechanical valves considering the prevalence of VHD among the young adults. The current hybrid valve is made of a non-degradable superelastic nitinol mesh scaffold, which is tightly enclosed by *in vitro* cultured tissue layers composed of three different cell types.[1] The present study explores how design features affect the dynamic characteristics of the tri-leaflet nitinol scaffold. These studies were performed to attain proper function in preparation of *in vivo* implantation. Multiple iterations in design and development of nitinol scaffolds were experimentally and computationally investigated until an acceptable design was achieved. The scaffolds were tested for preliminary hemodynamic performance and fatigue response in an accelerated wear testing system to determine the modes of failure. Moreover, to validate the scaffolds' structural response and mechanical integrity, a finite element model was introduced that computationally simulates the scaffolds' mechanical response under physiological pressure cycles. The computational method provides a powerful platform for design optimization and for investigating the fatigue response of the nitinol scaffold.

MATERIALS AND METHODS

Development of the Nitinol Scaffolds

To consider different key factors in the valve's structural design, several heart valve prototypes were made of nitinol mesh leaflets. Prior to assembling the valve scaffolds, the superelastic nitinol mesh leaflets were developed in two different shapes (Figs. 1a and 1b) through acid etching of flat annealed nitinol sheets (Johnson Matthey, PA, USA). According to the manufacturer, the sheets composed of nickel (55.70% by weight), titanium (>43.95%), and elements such as carbon and oxygen (<0.35%). The same data sheet reported the ultimate tensile strength as about 1000 MPa with 11.4% elongation. Our design comprises of a pattern of holes (240 μm diameter) on a square or hexagonal grid (center-to-center distance of 320 μm) that were etched over a 25 μm thick nitinol sheet. The etched sheets were shaped into desired size leaflets suited to make 21 mm heart valves (Figs. 1c and 1d). The mesh dimensions were chosen according to the sizes of the cells to be seeded over these scaffolds to make hybrid heart valves, as described previously.[1,2] Larger holes with diameters of 800 and 500 μm were considered on the leaflets' periphery to provide basal attachment and the commissures for sewing purposes, as shown in Figs. 1c and 1d, respectively. The leaflet boundaries in Figs. 1b and 1d contained a peripheral area with no holes. Three mesh leaflets of the same type were sewn into a valve frame to make a tri-leaflet nitinol valve scaffold. Multiple frames with different configurations were developed and tested as shown in Fig. 2 to identify the best design for our application. The frames were made through 3D printing of biocompatible Steralloy (Hapco, Hanover, MA; Fig. 2a), titanium (Solid Concepts, Valencia, CA; Fig. 2b), as well as titanium and PEEK (GPI Inc., IL, USA), as seen in Figs. 2c and 2d, respectively. The frames in Figs. 2c and 2d were complemented with three additional stands made of flexible polyethylene terephthalate (PET) to ensure the valve's posts allow for leaflet motion that is essential to the valve's opening and closure. All the frames were covered with and connected to the leaflets by biocompatible polyester surgical fabrics as shown in Fig. 3. Overall, two different design conditions were selected for further studies: first, the leaflets were connected to the frames/stands with no surgical fabric (Figs. 3a and 3b); and second, a thin layer of surgical fabric (C. R. Bard Inc., NJ, USA) connected the leaflets to the frames (Figs. 3c to 3e). For the groups with stands made of PET, they were sewn to the frame using thicker surgical fabrics to avoid buckling (Figs. 3e). The fabrics' thickness used to connect the leaflets to the frame/stands was 100 μm and the thickness of the fabrics connecting the stands to the frame was 1000 μm. The role of the fabric is to provide a soft connection between the frame/stands and the leaflets, thus allowing rotation and small translations that dampens high stress concentrations over the leaflet boundaries.

Durability and Hemodynamic Performance

To select the best design and to qualitatively check whether the nitinol scaffolds are compliant enough and can function similar to a heart valve, all the scaffolds shown in Fig. 3 were placed in a heart-pulsed duplicator system. The heart flow simulator system was adjusted for left ventricular pressure waveform with diastolic/systolic pressures of 80/120 mmHg produced by a hydraulic pump system (Superpump system, VSI, SPS3891, Vivitro systems Inc., Victoria, BC, Canada).[10] The scaffolds were placed at the aortic position inside a transparent silicone chamber that was made according to the human left ventricle. The waveforms were automatically adjusted according to

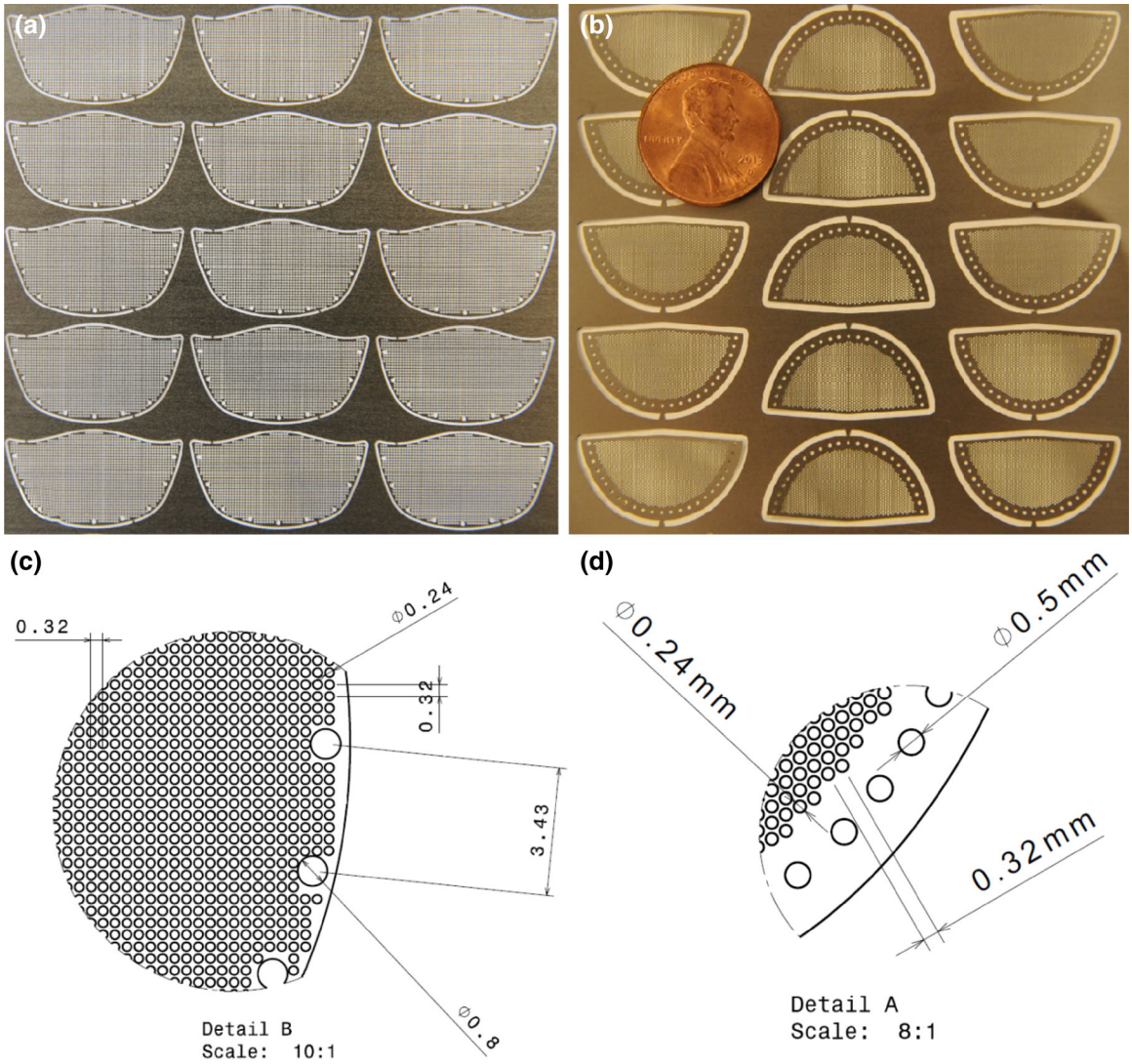

FIGURE 1. The superelastic nitinol mesh leaflets and their dimensions; geometries of the peripherally meshed (a) and the peripherally non-meshed (b) designs of the nitinol leaflets both made of 25 μm thick flat nitinol sheets. Dimensions of the central and side holes (for sewing purposes) for both peripherally meshed (c) and peripherally non-meshed (d) leaflets are shown.

the predefined heart rate and based on the position, velocity, and pressure feedbacks received by the power amplifier (VSI, SPA3891Z, Vivitro systems Inc., Victoria, BC, Canada) to produce a desired physiological flow regime inside the ventricular chamber.

Finally, the valve scaffold that qualitatively showed the best performance in the heart flow simulator ($n = 1$) was selected for further tests in a standard accelerated wear testing (AWT) system (Dynatek Labs, Galena, MO). The valve was tested for short-term durability analysis under 400, 600, and 800 cycles/min (cpm). This temperature-controlled AWT system contains saline and runs with system back pressure of 120 mmHg at 37 °C. The AWT system's harsh environment and high frequency pulsatile nature of the flow generate opening and closure of the nitinol scaffolds with inevitable leakage from the leaflet mesh holes. To partially resolve this, the leaflets were covered with a layer of polycarbonate die to seal the holes partially replicating the condition where cultured tissue encloses the mesh. The valve's opening area and the movements of the flexible posts were calculated using the ImageJ software and SketchAndCalc^{TM} online platform through analyzing the movie frames recorded during the course of these experiments. The test was performed far below one million cycles and did not mean to assess FDA-required standard fatigue response. The goal of this study was to find an initial improved design—considering the challenging design of this scaffold—so that the valves can be used for acute animal study.

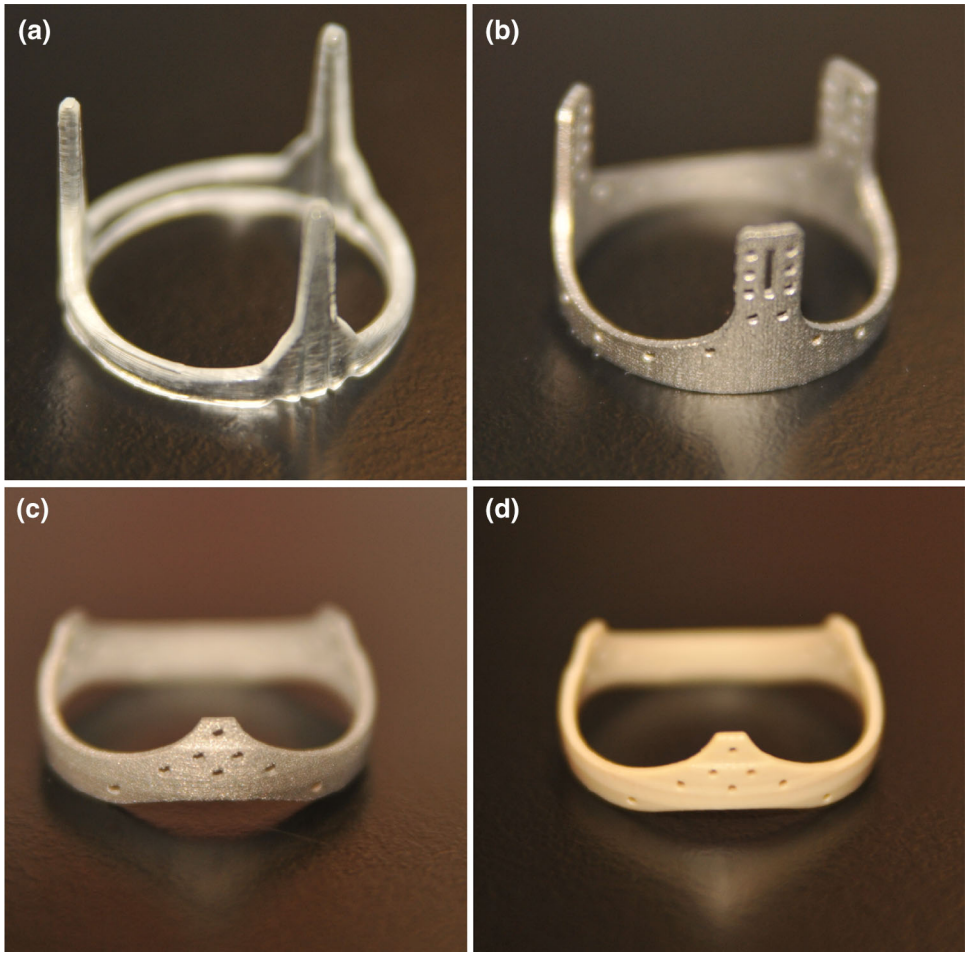

FIGURE 2. Heart valve frames that were used in this study made of Steralloy with uniformly attached fixed stands (a); titanium with fixed stands (b); titanium with separate stands (c); and PEEK with separate stands (d).

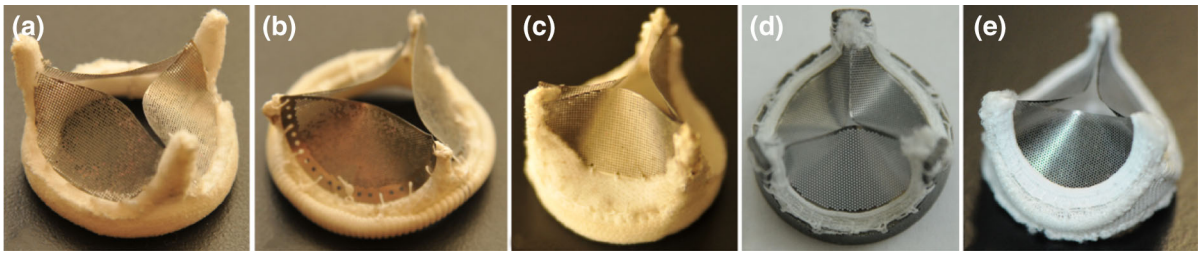

FIGURE 3. Tri-leaflet nitinol valve scaffolds comprised of multiple components made in two different categories; first group contained scaffolds with no fabrics between the leaflets and frame made of either uniform Steralloy frame using the peripherally meshed leaflets (a); or non-uniform frame with PET stands using the peripherally non-meshed leaflets (b). Second group contained scaffolds with fabrics between leaflets and frame/stands made of uniform Steralloy with peripherally meshed leaflets (c); uniform titanium with peripherally non-meshed leaflets (d); and non-uniform titanium with PET stands and peripherally non-meshed leaflets (e).

Synopsis of the Numerical Model

The mechanical response of the nitinol valve scaffold was modeled with the following procedure. First, the periodic configuration of the nitinol mesh leaflet was analyzed to extract its unit cell geometry (see Fig. 4a for all relevant dimensions). A numerical homogenization procedure[4] was used to extract the elastic properties of an effective homogeneous material from the mesh unit cell. Periodic boundary conditions were imposed to ensure that the effective properties be representative of the whole leaflet (Fig. 4b). Subse-

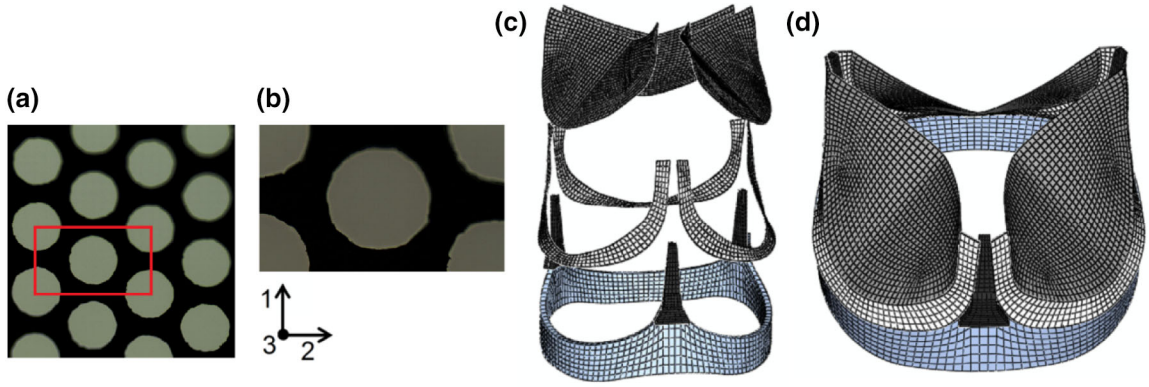

FIGURE 4. Sequential procedure for the structural analysis of the nitinol heart valve; (a) microstructure of the nitinol leaflet, (b) unit cell extracted from the nitinol leaflet's microstructure, (c) FEA modelling of the heart valve components comprising leaflets, fabrics, and frame with stands, and (d) FEA modelling of the entire assembly.

quently, the homogenized material properties were used to simulate the behavior of the curved leaflet in a finite element model of the entire scaffold. The commercial Finite Elements program Abaqus® (Dassault Systèmes, Vélizy, France) was used for all simulations. The other elements of the scaffold (stands, frame, and fabrics) were also modeled in connection with each other, as shown in Fig. 4c. Finally, the assembled model (Fig. 4d) was subjected to nonlinear dynamic analysis to study the time and spatial evolution of the stress distribution due to physiologic pressure differences (Fig. 5).

Extraction of a Homogenized Constitutive Model

Since the nitinol mesh is a very thin foil, only its in-plane elastic properties were considered. We used classic homogenization theory on a two-dimensional unit cell (Fig. 4b).[4] The effective (homogenized) elastic stiffness matrix of the mesh is expressed as:

$$C_{ij}^{H} = \frac{1}{A}\int_{A} C_{pq}\left(\epsilon_{p}^{0(i)} - \epsilon_{p}^{(i)}\right)\left(\epsilon_{q}^{0(j)} - \epsilon_{q}^{(j)}\right)\mathrm{d}A \qquad (1)$$

where C_{pq} is the local elastic stiffness matrix, $\epsilon^{0(i)}$ are three independent uniform unit-test strains $\left(\epsilon^{0(1)} = (1, 0, 0)^{\mathrm{T}}, \epsilon^{0(2)} = (0, 1, 0)^{\mathrm{T}}, \epsilon^{0(3)} = (0, 0, 1)^{\mathrm{T}}\right)$, $\epsilon^{(i)}$ is the local strain field corresponding to the application of each unit test strain, and A is the unit cell area. All indices vary between 1 and 3.

This problem was solved numerically, *via* the finite elements method described by Andreassen and Andreasen.[4] A rectangular unit cell was chosen to represent the hexagonal pattern (Fig. 4b), and discretized into a two-dimensional finite elements mesh. The stiffness matrix $\boldsymbol{k}_e$ of each element is expressed as:

$$\boldsymbol{k}_e = \int_{A_e} \boldsymbol{B}_e^{T}\boldsymbol{C}_e\boldsymbol{B}_e\mathrm{d}A_e \qquad (2)$$

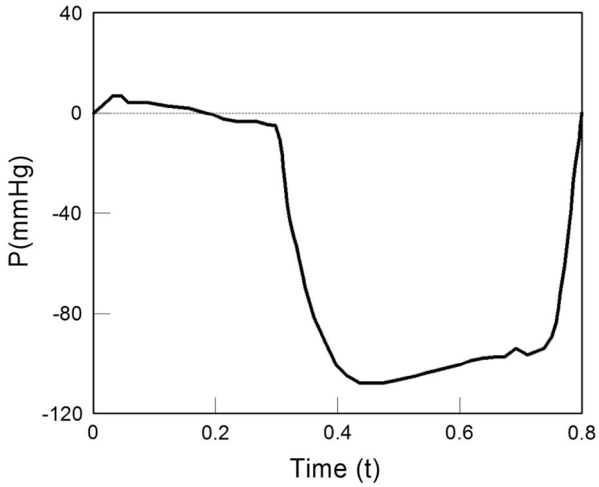

FIGURE 5. Physiological aortic transvalvular pressure profile applied to the leaflets during the explicit simulation, starting with an increasing opening pressure and followed by a decreasing closing pressure.

where $\boldsymbol{B}_e$ is the strain–displacement matrix and $\boldsymbol{C}_e$ is the element's stiffness matrix (Table 1). The integration was performed over the area of the element. The global stiffness matrix of the unit cell was calculated by the standard assembly procedure, such as $\boldsymbol{K} = \bigwedge_{e=1}^{N}\boldsymbol{k}_e$, with $\bigwedge$ denoting the assembly operator, and N the number of finite elements in the mesh. Equation (1) is expressed in discretized form as:

$$C_{ij}^{\mathrm{H}} = \frac{1}{A}\sum_{e=1}^{N}\left(\boldsymbol{d}_e^{0(i)} - \boldsymbol{d}_e^{(i)}\right)^{\mathrm{T}}\boldsymbol{k}_e\left(\boldsymbol{d}_e^{0(j)} - \boldsymbol{d}_e^{(j)}\right) \qquad (3)$$

where $\boldsymbol{d}_e^{0(i)}$ denotes the nodal displacement vector corresponding to the applied unit test strain, i.e., $\boldsymbol{B}_e\boldsymbol{d}_e^{0(i)} = \varepsilon^{0(i)}$, and $\boldsymbol{d}_e^{(i)}$ is the local displacement field obtained by solving three separate finite elements

TABLE 1. Material properties used in the computational modeling extracted from Šittner *et al.*,[35] Coble,[7] and Johnson Matthey Medical Components.[8]

	Nitinol	Polyester fabrics	PET	Homogenized nitinol
Young's modulus E (GPa)	75	0.2	3, 2, 0.5	14
Poisson's ratio (ν)	0.3	–	0.3	0.43
Density (kg/m^3)	6450	600	600	3225

problems, each with a force vector corresponding to one of the macroscopically applied test strains. The nodal force vectors can be assembled as:

$$\boldsymbol{f}^{(i)} = \bigwedge_{N}^{e=1} \boldsymbol{k}_e \boldsymbol{d}_e^{0(i)} \tag{4}$$

The nodal displacement vectors $\boldsymbol{d}^{(i)}$—consisting of the displacements $\boldsymbol{d}_e^{(i)}$ for each element—are then computed by solving the global matrix equation:

$$\boldsymbol{K}\boldsymbol{d}^{(i)} = \boldsymbol{f}^{(i)} \quad i = 1, \ldots, 3 \tag{5}$$

The homogenized stiffness matrix $\boldsymbol{C}^H$ can now be obtained from Eq. (3). The specific hexagonal symmetry of the unit cell under investigation (see Fig. 4b) implies isotropic mechanical response. Hence $\boldsymbol{C}^H$ has only two independent components, which can be expressed in terms of the common engineering constants: a Young's modulus, $E_{11} = E_{22}$, and a Poisson's ratio ($\nu_{12} = \nu_{21}$), relative to the coordinate system in Fig. 4b. The shear modulus G_{12} follows as $G_{12} = E_1/[2(1 + \nu_{12})]$. These moduli are extracted from the homogenized stiffness matrix as:

$$\left(\boldsymbol{C}^H\right)^{-1} = \begin{pmatrix} 1/E_1 & -\nu_{21}/E_1 & 0 \\ -\nu_{21}/E_1 & 1/E_1 & 0 \\ 0 & 0 & 1/G_{12} \end{pmatrix} \tag{6}$$

Table 1 provides the numerical values. This procedure was implemented in MATLAB (Mathworks, MA, USA) based on the algorithm defined by Andreassen and Andreasen.[4] We note that although the hexagonal mesh used in this work has isotropic stiffness, this procedure is universally applicable to meshes of any symmetry (or lack thereof).

Finite Element Analysis of the Scaffolds

All the scaffolds' geometries were developed in SolidWorks® (Dassault Systèmes, Vélizy, France) and all finite element simulations were performed in Abaqus® (Dassault Systèmes, Vélizy, France). The leaflet was modeled as a uniform, homogeneous and orthotropic thin shell (thickness of 25 μm) whose elastic properties were extracted from the numerical homogenization process as previously described (Table 1). The leaflet was meshed with 1110 linear elements (S4R) with reduced integration and enhanced hourglass control, to prevent excessive element distortion and well-known numerical inaccuracies; due to the very large rotations involved in the valve function, as well as the potentially large strain. Accordingly, a large-deformation finite-membrane strain solver was used for all simulations.[34] The supporting structures for the trileaflet scaffold, i.e. stands, fabrics, and frame, were simulated by using 180 solid hexagonal elements (C3D8R), 351 membrane elements (M3D4R), and a discrete rigid body, respectively. The fabrics and stands are made of polyester fibers and PET, respectively, with isotropic linear elastic material properties reported in Table 1.[7,8,35]

Typical polyester fabric has a modulus of ~2 GPa.[7] In the actual design, the fabric is only connected to the leaflets on discrete locations (the sewing points), a boundary condition that is difficult to properly model. In the context of this homogenized study, the finite elements model assumes perfect bonding of fabric and leaflet along the entire boundary; to compensate for the stiffer connection, the modulus of the fabric is reduced by ~1 order of magnitude, to a notional value of 0.20 GPa. Although this is certainly an approximate estimate, the general conclusions of this design study are not expected to be strongly influenced by small variations of this parameter. A physiologic transvalvular pressure wave was applied at a time-shifted aortic position, providing a positive opening pressure and a negative closing pressure over the leaflets (Fig. 5). A parametric study on the effect of leaflet thickness (ranging from 0.20 to 0.35 μm), stand stiffness ($E = 0.50$, 2.00, 3.00 GPa, and fully rigid), and fabric presence (fabric vs. no-fabric), on the valve response was performed.

RESULTS

Through our experiments, we learned three important concepts that are required to be considered for proper function of the nitinol scaffolds. First, the valve frames should be made of a durable material such as titanium with separate stands made of flexible materials such as PET to reduce the overall stress over the posts and to enhance opening and closure of the

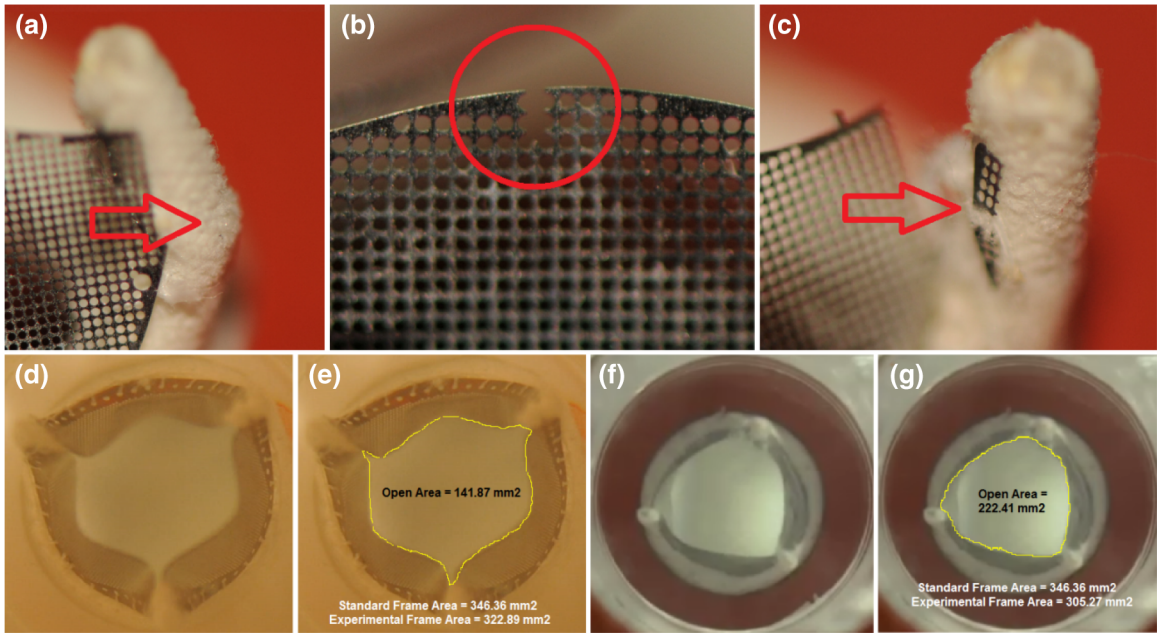

FIGURE 6. The nitinol valve scaffolds with no flexible posts or no interconnecting fabrics between their leaflets and frames and the ones with peripherally meshed leaflets showed unfavorable results during the preliminary tests. The test under 5 L/min flow rate inside a heart flow simulator led the fixed stands (a) and the tip (b) and sides (c) of the peripherally meshed leaflets to break. Additionally, lack of a thin fabric in between the leaflets and frame/stands resulted in extreme leaflet deflection during valve function (d) particularly during their maximum opening (e). The valve with no flexible posts and no interconnecting fabrics at its maximum opening phase (f) with the calculated open area is shown in (g).

valve's leaflets. Figure 6a shows how the valve's stands in Fig. 3a uniformly made of Steralloy frame (Fig. 2a) were damaged following a short-term test under 5 L/min flow rate inside the heart flow simulator. Second, the leaflets require a "no-hole" peripheral area at the basal attachment and at their free edges to avoid leaflet fracture due to excessive stress. Figures 6b and 6c show the fracture points in one of our earlier leaflet models, as shown of Fig. 1a, after a test in the heart flow simulator. Third, presence of a thin fabric in between the leaflets and frame/stands helps reducing the stress exerted over the leaflets by minimizing leaflet deflection during the valve function. Figure 6d shows testing of a nitinol scaffold with flexible stands but with no fabrics in between the frame/stands and among the leaflets. Even though, the leaflets were identical to the ones in Fig. 1b, the leaflet deflection was much higher, possibly due to the limited degrees of freedom, which may have resulted in leaflet rupture and valve failure in longer term experiments.

Relative Geometric Orifice Area and the Stands' Displacement

One parameter used to assess the valve performance is relative Geometric Orifice Area (GOA_r) evaluated in opening configuration as:

$$GOA_r = \frac{A_{open}}{A_{frame}} \tag{7}$$

where A_{open} and A_{frame} are the maximal cross-sectional area of the open valve at the leaflets' tip and enclosing frame's area, respectively. Frame's area can be calculated using either the ideal area of the circle based on the nominal valve diameter (standard GOA_r) or the actual area of the inflow circle (experimental GOA_r). Regardless, GOA_r ranges from 0 to 1, with the value of 1 corresponding to the largest opening similar to the no leaflet situation. The calculated standard and experimental GOA_rs for the valve in Fig. 6d are ~41 and ~44%, respectively, as shown in Fig. 6e. The maximum opening of the valve with no flexible posts and no interconnecting fabrics recorded during its function in heart flow simulator is also displayed in Fig. 6f. The standard and experimental GOA_rs were calculated and are reported in Fig. 6g as ~64 and ~73%, respectively. This GOA_r seems to be high enough but it may cause mechanical failure (Figs. 6a to 6c).

Figure 7 compares the dynamics of the experimental tests performed in the AWT system under 400, 600, and 800 cpm (Figs. 7a to 7c) using the nitinol tri-leaflet scaffold with flexible stands and interconnecting fabrics. From this comparison, we inferred that the nitinol valve under study opens and closes in a symmetric

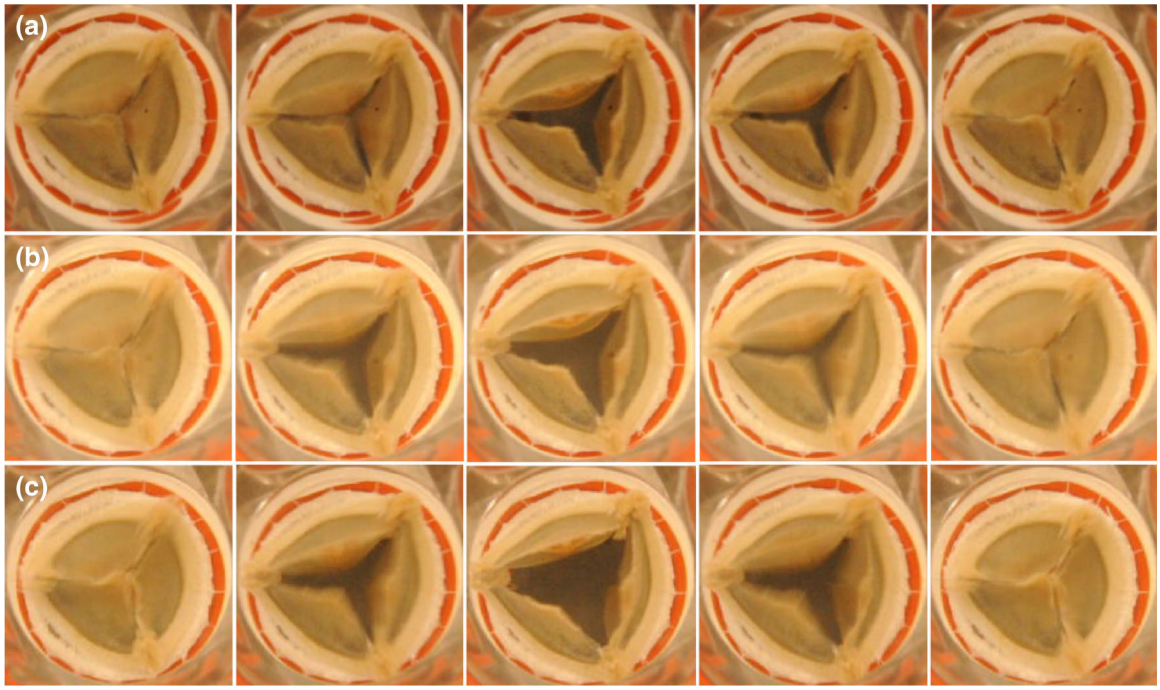

FIGURE 7. Comparison of the nitinol valve scaffolds function in an accelerated wear testing system under 400 (a); 600 (b); and 800 cpm (c) using scaffolds with flexible stands and interconnecting fabrics.

fashion. Figure 7 also qualitatively shows that using flexible posts and interconnecting fabrics would reduce leaflet deflection. The standard GOA_rs related to these tests in the AWT system are shown in Fig. 8 along with the horizontal displacement of the tip of the stands at different AWT speeds. The graph shows that both parameters increase as the speed increases. The GOA_r obtained from computer simulation was calculated as ~76% for a nitinol scaffold with similar characteristics as of the one shown in Fig. 7. This value is higher than the maximum standard GOA_r of ~44% (experimental GOA_r of ~52%) recorded in the AWT at 800cmp. A potential reason for this discrepancy is that the AWT systems are designed to replicate high cycles to rapidly test the valve's durability, and the GOA_r during the higher cycles may not accurately replicate the physiological and hemodynamic condition as the valve naturally operates. The other possible reason is the presence of a polymer coating that we used over the nitinol leaflets to cover the mesh holes. To be able to completely cover the middle gap available between the tips of the leaflets in closing position, the polymer coating was made sharp on the leaflets' tips similar to a triangle. This extra area added to the leaflets could have led to a smaller GOA_r as the computer simulation did not consider the coating. For the sake of comparison, the measured effective orifice area (EOA) under 5 L/min for a 21 mm commercially-available bioprosthetic heart valve made of bovine pericardium and porcine leaflets is ~1.48 and ~1.09 cm^2, respectively[14]. According to Garcia *et al.* for a funnel-shaped orifice (non-calcified native or bioprosthetic valves) the EOA almost equals to Geometric Orifice Area (GOA).[13] With this assumption, the standard GOA_rs can be calculated as ~42 and ~32% and the experimental GOA_rs as ~52 and ~48%, respectively. Additionally, if the internal tissue-annulus diameter is used to calculate their frame area[14] the GOA_rs would change to ~39 and ~32%, respectively. This should be mentioned that there might be slight differences between the area we have considered as the valve open area (GOA) with the definition of GOA in the prior references.

The computational model was used to study the dependence of the GOA_r on thickness of the nitinol leaflet. For the cases where fabric was used to connect the leaflets to the frame, the leaflet thickness of 35 μm allows for a GOA_r of ~73%, which can increase up to ~80% if the leaflet thickness is reduced to 20 μm. For the case in which the leaflets are directly connected to the frame without the fabric, the GOA_r barely exceeds 70% with a 25 μm thick leaflet. The stiffness of the stand seems not to significantly affect the GOA_r. However, it strongly affects the leaflet deformation during valve closure. An infinitely rigid stand would reduce the GOA_r to ~70% for the case of a 25- μm thick leaflet. With this GOA_r, the levels of stress experienced by the leaflets can be excessive. To accurately evaluate the performance of the valve designs, stress analysis is required, as described in the following section.

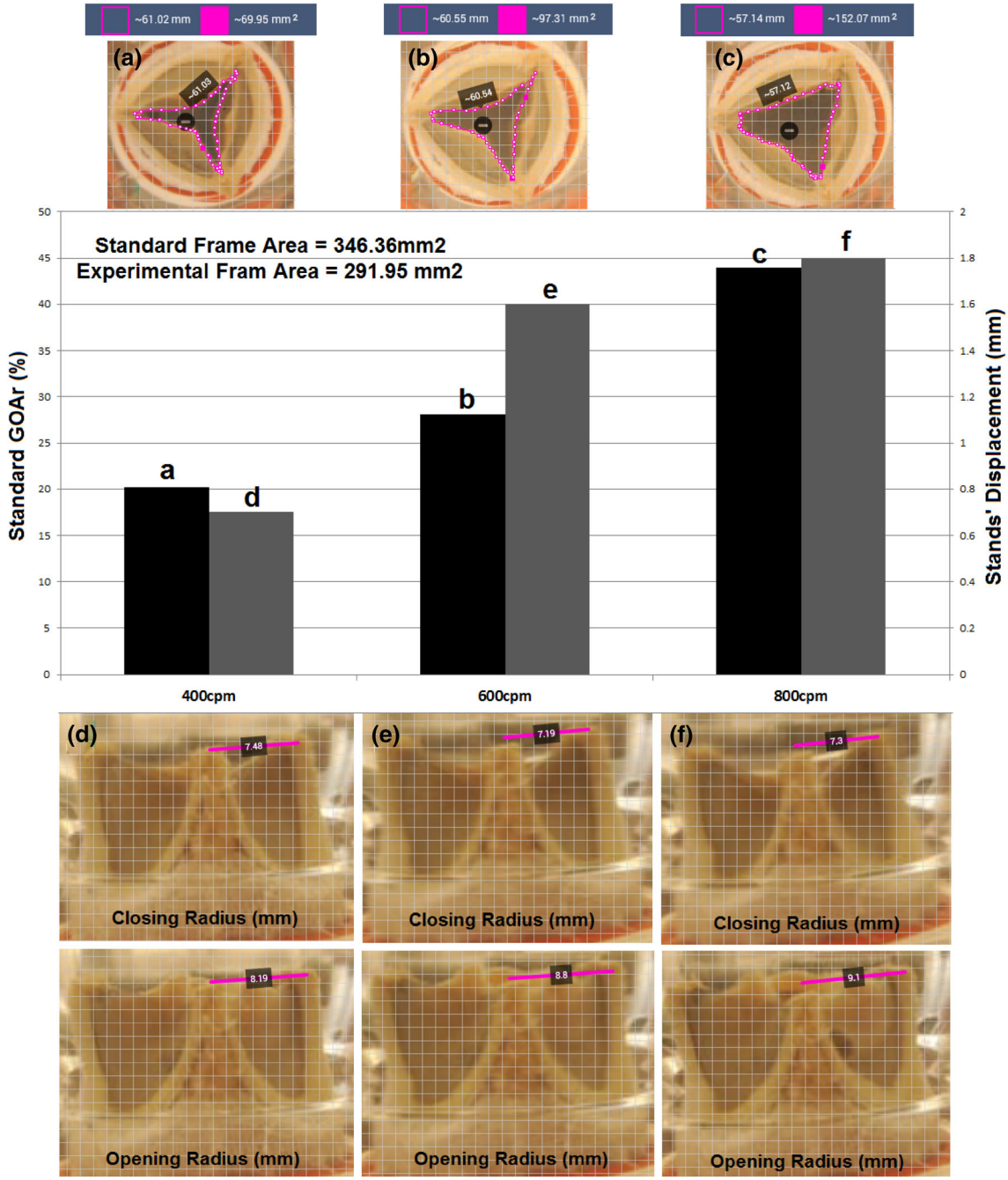

FIGURE 8. The extracted standard $GOA_r = \frac{A_{open}}{A_{frame}}$ (where A_{frame} is the ideal frame area and A_{open} is the GOA calculated based on the maximal open area at the leaflets' tip) and the horizontal displacement of the tip of the stands from the experiments performed in the AWT system at different speeds. Both parameters increase as the speed increases; (a) calculated open area for 400 cpm case and its correlated standard GOA_r, (b) calculated open area for 600 cpm case and its correlated standard GOA_r, (c) calculated open area for 800 cpm case and its correlated standard GOA_r, (d) calculated closing (top) and opening (bottom) radii for 400 cpm case and the associated displacement, (e) calculated closing (top) and opening (bottom) radii for 600 cpm case and the associated displacement, (f) calculated closing (top) and opening (bottom) radii for 800 cpm case and the associated displacement.

Stress Analysis

The level of stress experienced by the leaflets directly affects valve durability. We computed the spatial and temporal evolutions of the equivalent (von Mises) stress, σ_{eq}, for different design configurations. This choice is appropriate, as the hexagonal symmetry of

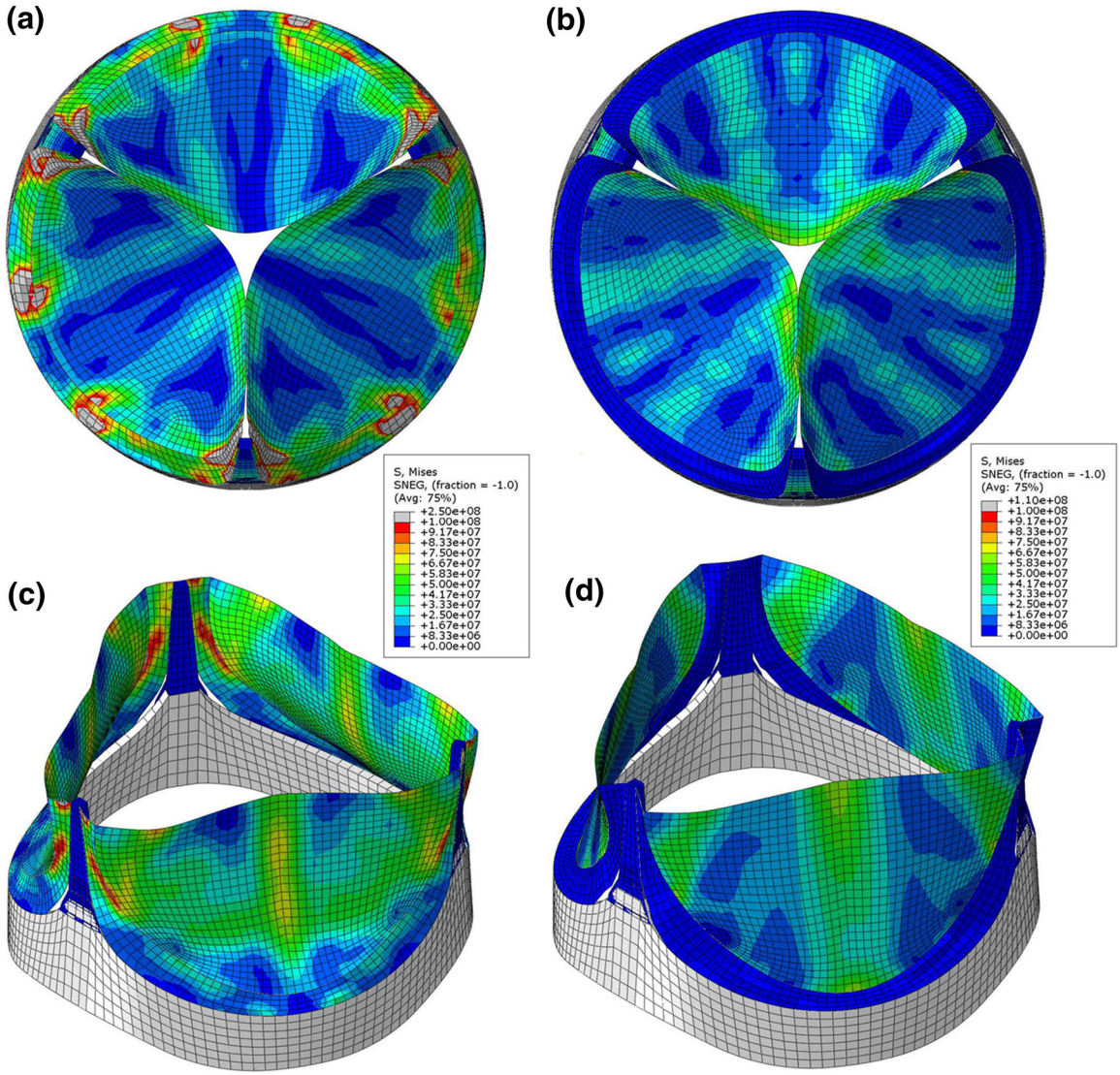

FIGURE 9. Von Mises stresses on the nitinol leaflets at the instant of maximum negative pressure (closed configuration) and maximum positive pressure (open configuration) for when the leaflets are connected to the frame without fabrics (a and c) and with fabrics (b and d), respectively.

the pattern of holes in the leaflet implies that the effective material behaves isotropically. It can be observed in Fig. 9 that the equivalent stress dramatically increases if no fabric is used to connect the leaflets to the frame. Figure 9a shows that in absence of the fabric, a maximum equivalent stress of ~250 MPa is reached during closure in the leaflets near the attachment to the frame. However, if the fabric is used to connect the leaflets to the frame, this value drops to ~110 MPa, and is localized to the free edges of the leaflets (Fig. 9b). During opening, the maximum stresses are lower: ~115 MPa in the absence of the fabric (Fig. 9c) and ~80 MPa in presence of the fabric (Fig. 9d). The presence of the fabric will be assumed from this point on.

Not surprisingly, the stress distribution is also a strong function of the leaflet thickness. The numerical values of the maximum von Mises stresses upon opening and closure are reported in Fig. 10. In all cases, the maximum stress occurs during closure and is associated with contact of the leaflet edges. For the smallest considered thickness of 20 μm, the maximum stress is very large (~190 MPa); but it drops significantly as the thickness increases (down to ~90 MPa for a thickness of 35 μm).

Figure 11 illustrates the dependence of the stress distribution within the leaflet on the stiffness of the stands. A compliant stand allows for more leaflet deformation, and hence more contact during closing, which generally results in higher stresses. The maxi-

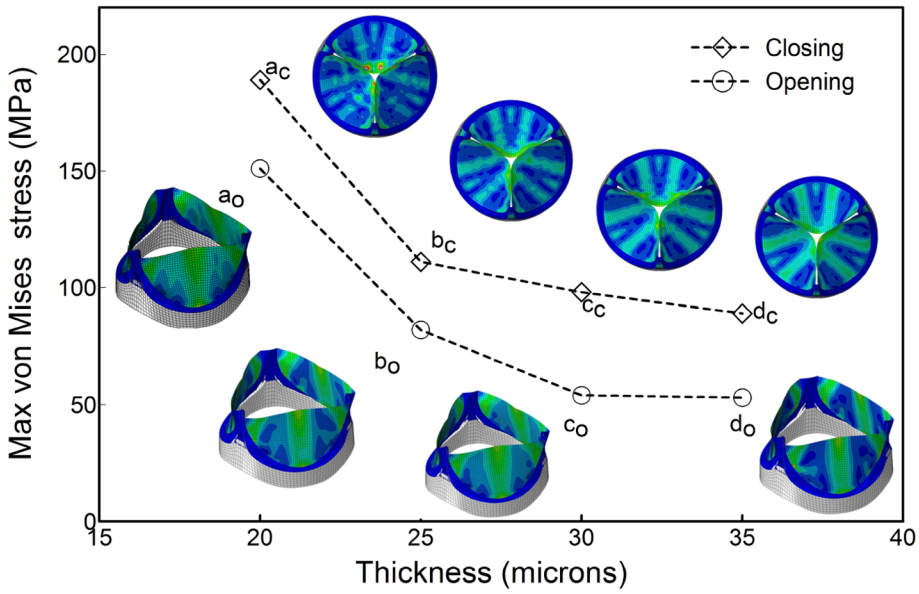

FIGURE 10. Maximum von Mises stresses on the nitinol leaflets at the instant of maximum negative pressure (closing, "c") and maximum positive pressure (opening, "o") for leaflet thicknesses of (a) 20 μm; (b) 25 μm; (c) 30 μm; and (d) 35 μm.

mum equivalent stress in a nitinol valve with a stand's Young's modulus of 0.5 GPa is ~250 MPa, whereas for a stand with Young's modulus of 2 and 3 GPa, the maximum stresses drop to ~150 and ~110 MPa, respectively. Beyond a given value of the modulus, the stand becomes sufficiently stiff to overcome significant contact among the leaflets upon closure, at which point the magnitude of the maximum stress becomes largely unaffected by the modulus of the stand. For fully rigid stands, a maximum equivalent stress of ~120 MPa is located in vicinity of the stands (Fig. 11d).

Unit Cell Stresses and Fatigue Life

The stress distributions discussed in the previous section refer to the homogenized leaflet. The actual stresses in the elements of the nitinol mesh will be much higher, and these local stresses must be extracted and compared to the material's yield stress (or its fatigue limit) to assess the structural integrity of the leaflet. An estimate of the local stress distribution in the nitinol mesh can be obtained with a finite element model of its unit cell. A two-dimensional model with plane stress conditions can be justified to use because the leaflet is a thin shell with bending stresses much smaller than the membrane stresses. This was verified by comparing the stress values on the top and bottom side of the leaflet: the average difference was found 4.5% with a peak value of 12.3%. The full valve model with homogenized leaflets described in the previous section was used to identify the magnitude of the peak in-plane strain components, which generally occurs at the location where the effective von Mises stress is the maximum. These strain components were subsequently imposed as boundary conditions on the unit cell model, and the local stresses are extracted. To simplify the application of periodic boundary conditions, two separate models were run: one in which the axial strains ε_{11} and ε_{22} were applied as boundary conditions (with no shear strain, ε_{12}), and the other one in which the shear strain ε_{12} was applied alone. From each model, the in-plane stress components σ_{11}, σ_{12} and σ_{12} were extracted. Linear elasticity allows superposition of the individual stress components from the two models, resulting in the overall local stress distributions. The equivalent von Mises stress can then be calculated and the peak equivalent stress used for design considerations. For the design configuration where the stands have a Young's modulus of 3 GPa with the leaflets having a thickness of 25 μm (resulting in a maximum homogenized stress of ~ 110 MPa), a maximum local von Mises stress of ~390 MPa was extracted. This value represents the largest stress experienced by the nitinol mesh at any given location and time, and can be compared to the yield strength of nitinol to assess the structural viability of the leaflets. As the yield strength of nitinol is 560 MPa, the leaflets for this specific design configuration are in a safe region.[22]

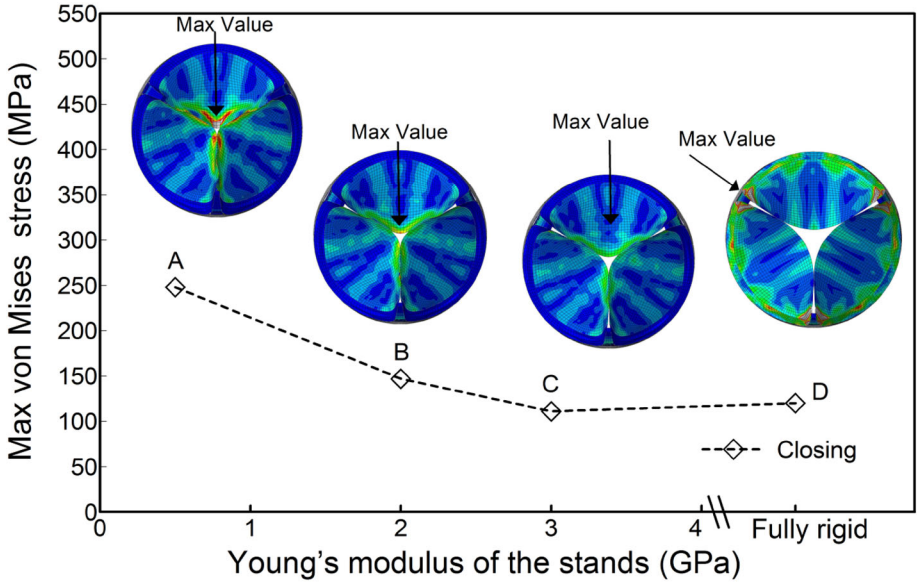

FIGURE 11. Maximum von Mises stresses on the nitinol leaflets at the instant of maximum negative pressure (closed configuration) for the stands with the Young's modulus of (a) 500 MPa; (b) 2000 MPa, (c) 3000 MPa, and for the fully rigid case (d).

DISCUSSION

We have implemented experimental testing and computational modeling to assess and optimize different design parameters for a novel tri-leaflet nitinol mesh scaffold. This non-degradable scaffold can act as a permanent load bearing component potentially eliminating the leaflet shrinkage risks associated with degradable scaffolds used for TEHVs. The scaffold has the potential to be used for *in vivo*, *in situ*, and off-the-shelf tissue engineering approaches. It has been shown that the suboptimal valve design may result in abnormal valve function due to many reasons such as incomplete coaptation, inadequate or excessive opening, asymmetric stress distribution, mechanical rupture, and abnormally high stresses throughout the scaffold.[9,11,19,20,38,41] Computational simulation, in parallel with experimental studies, has been extensively used in the last two decades to assess and to predict the function and mechanics of heart valves *in vitro* prior to implantation.[17] These studies have investigated native and prosthetic heart valves in normal and diseased conditions and have assisted in analysis of their function and design. The accuracy of *in vitro* experimental and computational analysis is highly dependent on the factors such as valve geometry and components, material properties, and the loading and boundary conditions.

The present work studies the function of a tri-leaflet mesh scaffold valve experimentally and computationally to test the effect of various geometric and materials parameters on its performance. This led to an improved scaffold design with minimal stresses over the leaflets and potentially improved fatigue life. To correctly simulate the leaflets and their fine-scale mesh structure while maintaining reasonable computational speed, we adopted an elastic homogenization technique to extract effective properties of the leaflet and used these parameters in a dynamic finite elements model for the full valve. The homogenization step was crucial, as the element size required to capture the details between consecutive holes in each mesh leaflet was far too small for a model of the entire valve.

We noticed that a large variety of constitutive models have been used in the literature to characterize the valve tissue properties, ranging from linear elastic models,[6,18,25] to Fung-elastic models,[36] and strain invariant-based hyperelastic approaches.[26,42] These models are unnecessary for the nitinol leaflets analyzed in this work, as nitinol largely behaves as a linear elastic material over the range of strains experienced in this application. The high stiffness of the nitinol can be compensated by choosing sufficiently thin leaflets and properly designing the valve scaffold in connection with the leaflets. Our results indicate that the peak stresses experienced by the leaflets are observed during valve closure due to the contact between the free edges of the nitinol leaflets that creates large strains. Carefully choosing appropriate stand and leaflet stiffness/thickness will minimize the contact, and therefore, reduce the stresses over each leaflet and would lead to a larger GOA_r. Our model reveals that the stand's Young's modulus of 3 GPa along with the leaflet thickness of 25 μm currently provides the best results for our application. However, since the valves are

manually sewn, a heterogeneity among the valves' function are anticipated. It should be mentioned that a small gap between the free edges of the leaflets in the stress-free state of the scaffolds (closed condition) will ultimately be filled by the cultured tissue that surrounds the meshes. This will probably eliminate—or at least minimize—the direct contact between the leaflets and should dramatically reduce the contact stresses.

Our model also revealed that the presence of a surgical fabric layer connecting the nitinol leaflets to the frame is essential for proper operation of the valve. Even though the durability/fatigue test performed in this study cannot be considered standard or definitive due to the mesh leakage and coating limitations, the AWT experiments provided valuable information on how the nitinol scaffold performs under high cycle tests at different frequencies. Our results showed that the GOA_r improves at higher frequencies. Connecting the leaflets to the rigid frame without using the intermediary fabric would result in leaflets' commissures not achieving a complete closed configuration during the valve closure as well as dramatically elevated stress values. For the improved design, the peak local von Mises stress in the leaflet was ~390 MPa. This stress is considerably lower than both the yield strength of nitinol (~560 MPa) and comparable to its reported[29] fatigue threshold (~400 MPa), suggesting that the leaflets should resist long-term fatigue. Based on this assessment, a fatigue life expectancy in excess of 10^7 cycles can be estimated. We emphasize that this estimate is likely to be conservative, as the local maximum stress in the leaflet will be reduced by the presence of the living tissue coating. Finally, we anticipate that the presence of a live tissue covering the mesh holes would provide a leakage-free surface that requires minimal forces for opening, as seen in our experimental data.

A limitation of this study is that only one valve was tested under AWT system. Therefore, reproducibility of the experimental results is neither guaranteed nor tested, and may change since the valves are manually sewn and even slight variation in sewing may generate large discrepancy. However, the purpose of this study was only to improve the valve function and to minimize the stresses by modeling different conditions for valve's components.

Comprehensive assessment of the function of these scaffolds requires perfect coating of the scaffolds with live cells and testing them in a bioreactor that completely resembles the *in vivo* situation and provides all the mechanical and biological factors. These bioreactors need to provide the migratory and circulatory cell remodeling mechanisms as well. The remodeling will eventually change the leaflets' geometry and affects the hemodynamics. In addition, the pressures and exact *in vivo* geometry of the heart chambers are difficult to simulate. Designing such a bioreactor is a challenging task and may be even more difficult than *in vivo* experimentation. Therefore, the experimental results of this study should be considered as a preliminary hemodynamic assessment.

ACKNOWLEDGMENTS

This work was supported by a grant from Children's Heart Foundation to Prof. Kheradvar and a postdoctoral grant from American Heart Association (16POST27540025) to Dr. Alavi. There are no financial disclosures.

REFERENCES

[1]Alavi, S. H., and A. Kheradvar. Metal mesh scaffold for tissue engineering of membranes. *Tissue Eng. Part C Methods* 18:293–301, 2011.
[2]Alavi, S. H., and A. Kheradvar. A hybrid tissue-engineered heart valve. *Ann. Thoracic Surg*. 99:2183–2187, 2015.
[3]Alavi, S. H., W. F. Liu, and A. Kheradvar. Inflammatory response assessment of a hybrid tissue-engineered heart valve leaflet. *Ann. Biomed. Eng*. 41:316–326, 2013.
[4]Andreassen, E., and C. S. Andreasen. How to determine composite material properties using numerical homogenization. *Comput. Mater. Sci*. 83:488–495, 2014.
[5]Bouten, C., P. Dankers, A. Driessen-Mol, S. Pedron, A. Brizard, and F. Baaijens. Substrates for cardiovascular tissue engineering. *Adv. Drug Deliv. Rev*. 63:221–241, 2011.
[6]Cataloglu, A., R. E. Clark, and P. L. Gould. Stress analysis of aortic valve leaflets with smoothed geometrical data. *J. Biomech*. 10:153–158, 1977.
[7]Coble, S. Materials Data Book. Cambridge: Cambridge University Engineering Department, 2003.
[8]Database JMC. An overview of nitinol: Superelastic and shape memory. *Medical Design Briefs*. 2015.
[9]Driessen-Mol, A., M. Y. Emmert, P. E. Dijkman, L. Frese, B. Sanders, B. Weber, N. Cesarovic, M. Sidler, J. Leenders, and R. Jenni. Transcatheter implantation of homologous "off-the-shelf" tissue-engineered heart valves with self-repair capacity: long-term functionality and rapid *in vivo* remodeling in sheep. *J. Am. Coll. Cardiol*. 63:1320–1329, 2014.
[10]Falahapisheh, A., and A. Kheradvar. High-speed particle image velocimetry to assess cardiac fluid dynamics *in vitro*: From performance to validation. *Eur. J. Mech. B/Fluids* 35:2–8, 2012.
[11]Fan, R., A. S. Bayoumi, P. Chen, C. M. Hobson, W. R. Wagner, J. E. Mayer, and M. S. Sacks. Optimal elastomeric scaffold leaflet shape for pulmonary heart valve leaflet replacement. *J. Biomech*. 46:662–669, 2013.
[12]Flanagan, T. C., J. S. Sachweh, J. Frese, H. Schnöring, N. Gronloh, S. Koch, R. H. Tolba, T. Schmitz-Rode, and S. Jockenhoevel. *in vivo* remodeling and structural characterization of fibrin-based tissue-engineered heart valves in the adult sheep model. *Tissue Eng. Part A* 15:2965–2976, 2009.
[13]Garcia, D., P. Pibarot, C. Landry, A. Allard, B. Chayer, J. G. Dumesnil, and L.-G. Durand. Estimation of aortic valve

effective orifice area by doppler echocardiography: effects of valve inflow shape and flow rate. *J. Am. Soc. Echocardiogr.* 17:756–765, 2004.
[14]Gerosa, G., V. Tarzia, G. Rizzoli, and T. Bottio. Small aortic annulus: the hydrodynamic performances of 5 commercially available tissue valves. *J. Thoracic Cardiovasc. Surg.* 131(1058–1064):e1052, 2006.
[15]Hoerstrup, S. P., R. Sodian, S. Daebritz, J. Wang, E. A. Bacha, D. P. Martin, A. M. Moran, K. J. Guleserian, J. S. Sperling, and S. Kaushal. Functional living trileaflet heart valves grown *in vitro*. *Circulation* 102:Iii-44–Iii-49, 2000.
[16]Kheradvar, A., E. M. Groves, L. P. Dasi, S. H. Alavi, R. Tranquillo, K. J. Grande-Allen, C. A. Simmons, B. Griffith, A. Falahatpisheh, and C. J. Goergen. Emerging trends in heart valve engineering: part I. Solutions for future. *Ann. Biomed. Eng.* 43:833–843, 2015.
[17]Kheradvar, A., E. M. Groves, A. Falahatpisheh, M. K. Mofrad, S. H. Alavi, R. Tranquillo, L. P. Dasi, C. A. Simmons, K. J. Grande-Allen, and C. J. Goergen. Emerging trends in heart valve engineering: part IV. Computational modeling and experimental studies. *Ann. Biomed. Eng.* 43:2314–2333, 2015.
[18]Kunzelman, K., R. Cochran, C. Chuong, W. Ring, E. Verrier, and R. Eberhart. Finite element analysis of the mitral valve. *J. Heart Valve Dis.* 2:326–340, 1993.
[19]Labrosse, M. R., C. J. Beller, F. Robicsek, and M. J. Thubrikar. Geometric modeling of functional trileaflet aortic valves: Development and clinical applications. *J. Biomech.* 39:2665–2672, 2006.
[20]Loerakker, S., G. Argento, C. W. Oomens, and F. P. Baaijens. Effects of valve geometry and tissue anisotropy on the radial stretch and coaptation area of tissue-engineered heart valves. *J. Biomech.* 46:1792–1800, 2013.
[21]Loger, K., A. Engel, J. Haupt, R. L. de Miranda, G. Lutter, and E. Quandt. Microstructured nickel-titanium thin film leaflets for hybrid tissue engineered heart valves fabricated by magnetron sputter deposition. *Cardiovasc. Eng. Technol.* 7:69–77, 2016.
[22]McKelvey, A., and R. Ritchie. Fatigue-crack propagation in nitinol, a shape-memory and superelastic endovascular stent material. *J. Biomed. Mater. Res.* 47:301–308, 1999.
[23]Mol, A., A. I. Smits, C. V. Bouten, and F. P. Baaijens. Tissue engineering of heart valves: advances and current challenges. *Exp. Rev. Med. Dev.* 6:259–275, 2009.
[24]Mozaffarian, D., E. J. Benjamin, A. S. Go, D. K. Arnett, M. J. Blaha, M. Cushman, S. R. Das, S. de Ferranti, J.-P. Després, and H. J. Fullerton. Heart disease and stroke statistics—2016 update a report from the American heart association. *Circulation* 133(4):447, 2015; (CIR. 0000000000000350).
[25]Pouch, A. M., C. Xu, P. A. Yushkevich, A. S. Jassar, M. Vergnat, J. H. Gorman, R. C. Gorman, C. M. Sehgal, and B. M. Jackson. Semi-automated mitral valve morphometry and computational stress analysis using 3d ultrasound. *J. Biomech.* 45:903–907, 2012.
[26]Prot, V., B. Skallerud, G. Sommer, and G. A. Holzapfel. On modelling and analysis of healthy and pathological human mitral valves: two case studies. *J. Mech. Behav. Biomed. Mater.* 3:167–177, 2010.
[27]Reimer, J., Z. Syedain, B. Haynie, M. Lahti, J. Berry, and R. Tranquillo. Implantation of a tissue-engineered tubular heart valve in growing lambs. *Ann Biomed Eng* 2016. doi: 10.1007/s10439-016-1605-7.
[28]Reshetov, I., O. Starceva, A. Istranov, B. Vorona, A. Lyundup, I. Gulyaev, D. Melnikov, D. Shtansky, A. Sheveyko, V. Andreev. Three-dimensional biocompatible matrix for reconstructive surgery. *Physics Of Cancer: Interdisciplinary Problems And Clinical Applications (Pc'16): Proceedings of the International Conference on Physics of Cancer: Interdisciplinary Problems and Clinical Applications 2016*. 1760: 020056, 2016.
[29]Robertson, S., A. Pelton, and R. Ritchie. Mechanical fatigue and fracture of nitinol. *Int. Mater. Rev.* 57:1–37, 2012.
[30]Ruiz, C. E., M. Iemura, S. Medie, P. Varga, W. G. Van Alstine, S. Mack, A. Deligio, N. Fearnot, U. H. Beier, and D. Pavcnik. Transcatheter placement of a low-profile biodegradable pulmonary valve made of small intestinal submucosa: a long-term study in a swine model. *J. Thorac Cardiovasc. Surg.* 130:e471–e477, 2005.
[31]Sanders, B., S. Loerakker, E. S. Fioretta, D. J. Bax, A. Driessen-Mol, S. P. Hoerstrup, and F. P. Baaijens. Improved geometry of decellularized tissue engineered heart valves to prevent leaflet retraction. *Ann. Biomed. Eng.* 44:1061–1071, 2016.
[32]Schmidt, D., P. E. Dijkman, A. Driessen-Mol, R. Stenger, C. Mariani, A. Puolakka, M. Rissanen, T. Deichmann, B. Odermatt, and B. Weber. Minimally-invasive implantation of living tissue engineered heart valves: a comprehensive approach from autologous vascular cells to stem cells. *J. Am. Coll. Cardiol.* 56:510–520, 2010.
[33]Shinoka, T., C. K. Breuer, R. E. Tanel, G. Zund, T. Miura, P. X. Ma, R. Langer, J. P. Vacanti, and J. E. Mayer. Tissue engineering heart valves: valve leaflet replacement study in a lamb model. *Ann. Thorac. Surg.* 60:S513–S516, 1995.
[34]Shinoka, T., P. X. Ma, D. Shum-Tim, C. K. Breuer, R. A. Cusick, G. Zund, R. Langer, J. P. Vacanti, and J. E. Mayer, Jr. Tissue-engineered heart valves. Autologous valve leaflet replacement study in a lamb model. *Circulation* 94:II164–II168, 1996.
[35]Šittner, P., L. Heller, J. Pilch, C. Curfs, T. Alonso, and D. Favier. Young's modulus of austenite and martensite phases in superelastic niti wires. *J. Mater. Eng. Perform.* 23:2303–2314, 2014.
[36]Sun, W., A. Abad, and M. S. Sacks. Simulated bioprosthetic heart valve deformation under quasi-static loading. *J. Biomech. Eng.* 127:905–914, 2005.
[37]Sutherland, F. W., T. E. Perry, Y. Yu, M. C. Sherwood, E. Rabkin, Y. Masuda, G. A. Garcia, D. L. McLellan, G. C. Engelmayr, and M. S. Sacks. From stem cells to viable autologous semilunar heart valve. *Circulation* 111:2783–2791, 2005.
[38]Swanson, W. M., and R. E. Clark. Dimensions and geometric relationships of the human aortic value as a function of pressure. *Circ. Res.* 35:871–882, 1974.
[39]Syedain, Z. H., M. T. Lahti, S. L. Johnson, P. S. Robinson, G. R. Ruth, R. W. Bianco, and R. T. Tranquillo. Implantation of a tissue-engineered heart valve from human fibroblasts exhibiting short term function in the sheep pulmonary artery. *Cardiovasc. Eng. Technol.* 2:101–112, 2011.
[40]Syedain, Z., J. Reimer, J. Schmidt, M. Lahti, J. Berry, R. Bianco, and R. T. Tranquillo. 6-month aortic valve implantation of an off-the-shelf tissue-engineered valve in sheep. *Biomaterials* 73:175–184, 2015.
[41]Thubrikar, M., W. C. Piepgrass, T. W. Shaner, and S. P. Nolan. The design of the normal aortic valve. *Am. J. Physiol. Heart Circ. Physiol.* 241:H795–H801, 1981.
[42]Wang, Q., and W. Sun. Finite element modeling of mitral valve dynamic deformation using patient-specific multi-slices computed tomography scans. *Ann. Biomed. Eng.* 41:142–153, 2013.